Modeling Cavitation in a Rapidly Changing Pressure Field – Application to a Small Ultrasonic Horn

Anton Žnidarčič, Robert Mettin, Matevž Dular

PII: S1350-4177(14)00170-9
DOI: http://dx.doi.org/10.1016/j.ultsonch.2014.05.011
Reference: ULTSON 2607

To appear in: *Ultrasonics Sonochemistry*

Received Date: 14 October 2013
Revised Date: 8 May 2014
Accepted Date: 16 May 2014

Please cite this article as: A. Žnidarčič, R. Mettin, M. Dular, Modeling Cavitation in a Rapidly Changing Pressure Field – Application to a Small Ultrasonic Horn, *Ultrasonics Sonochemistry* (2014), doi: http://dx.doi.org/10.1016/j.ultsonch.2014.05.011

Modeling Cavitation in a Rapidly Changing Pressure Field – Application to a Small Ultrasonic Horn

Anton Žnidarčič
Laboratory for Water and Turbine Machines
University of Ljubljana
Aškerčeva 6, 1000 Ljubljana, Slovenia

Robert Mettin
Christian Doppler Laboratory for Cavitation and Micro-Erosion,
Drittes Physikalisches Institut
Universität Göttingen
Friedrich-Hund-Platz 1, 37077 Göttingen, Germany

Matevž Dular (corresponding author)
Laboratory for Water and Turbine Machines
University of Ljubljana
Aškerčeva 6, 1000 Ljubljana, Slovenia

Abstract
Ultrasonic horn transducers are frequently used in applications of acoustic cavitation in liquids. It has been observed that if the horn tip is sufficiently small and driven at high amplitude, cavitation is very strong, and the tip can be covered entirely by the gas/vapour phase for longer time intervals. A peculiar dynamics of the attached cavity can emerge with expansion and collapse at a self-generated frequency in the subharmonic range, i.e. below the acoustic driving frequency. The term "acoustic supercavitation" was proposed for this type of cavitation [1].
We tested several established hydrodynamic cavitation models on this problem, but none of them was able to correctly predict the flow features. As a specific characteristic of such acoustic cavitation problems lies in the rapidly changing driving pressures, we present an improved approach to cavitation modeling, which does not neglect the second derivatives in the Rayleigh-Plesset equation. Comparison with measurements of acoustic supercavitation at an ultrasonic horn of 20 kHz frequency revealed a good agreement in terms of cavity dynamics, cavity volume and emitted pressure pulsations.
The newly developed cavitation model is particularly suited for simulation of cavitating flow in highly fluctuating driving pressure fields.

Key words: Cavitation, ultrasonic horn, Rayleigh-Plesset equation, CFD, acoustic supercavitation

List of symbols

C_{dest}	coefficient of vapour destruction
C_{prod}	coefficient of vapour production
f_g	non-condensable gas mass fraction
f_v	vapour mass fraction
k	turbulent kinetic energy
n_0	bubble number density
R	bubble radius
R_0	initial bubble radius
S_{dest}	source term of vapour destruction
S_{prod}	source term of vapour production

p_{g0} initial gas pressure
p_v vapour pressure
p_∞ pressure in far field
T_b bubble temperature
T_∞ temperature in far field
t_∞ mean flow time scale
u velocity
u_g grid velocity
u_{mo} modified velocity
u_{or} original velocity
u_∞ velocity in far field
α volume fraction
α_l liquid volume fraction
α_{nuc} nucleation site volume fraction
α_v vapour volume fraction
Δt length of a time step
μ dynamic viscosity
ρ_l liquid density
ρ_m mixture density
ρ_v vapour density
σ surface tension
Φ general scalar

1 Introduction

Cavitation occurs in very different situations and is denoted as the process of a breakdown of a homogeneous liquid medium under very low pressures and a consequent collapse of vapour bubbles when the pressure is elevated. In liquid flows, this phase change is generally due to local high velocities which induce low pressures. The liquid medium is then "broken" at one or several points and "voids" appear, whose shape depends strongly on the structure of the flow. However, cavitation can also occur in a static or nearly static liquid. When an oscillating pressure field is applied over the free surface of a liquid contained in a reservoir, cavitation bubbles may appear within the liquid bulk if the oscillation amplitude is large enough. This type of cavitation is known as acoustic cavitation [2].

Numerical simulation of cavitating flows and specifically the development of phase change models has received enormous attention from researchers during the last years. Early studies, that primarily utilized the potential flow theory, are still widely used in engineering applications. Most of the codes treat the two phase flow as a single vapour-liquid phase mixture flow. An exception is for example a numerical study of cavitating flow in the nozzle performed by Alajbegovic et al. [3], where each phase was separately modeled.

In the simplest approach it is assumed that the flow is seeded by cavitation nuclei. Usually a simplified Rayleigh-Plesset equation is used to determine the change in bubble size and consequently the mixture density in each computational cell. The advantage of this formulation is that it follows, to some part, a physical law. However one neglects the hydrodynamics of the vapour phase and overpredicts the vapour volume fraction – especially in cases of cloud cavitation. This approach was first introduced by Kubota et al. [4] who used the linear part in the Rayleigh-Plesset equation to describe the evolution of bubble radius as a function of the surrounding pressure.

A different approach was proposed by several authors [5-13] in form of essentially the same transport equation models. In their approach volume or mass fraction of liquid (and vapour) phase is convected. This method has the advantage that it can take into account the time influence on the mass transfer phenomena through empirical laws for the source term. One clear advantage of models from this family comes from the convective character of the equation that allows modeling of the impact of inertial forces on cavities like elongation, detachment and drift of bubbles.

Another way to model cavitation processes is by the so called barotropic state law that links the density of vapour-liquid mixture to the local static pressure. The model was proposed by Delannoy & Kueny [14] and later widely used by others [15-18]. The results obtained with the barotropic cavitation model show very good correlation to the experiments but past simulations lacked robustness of numerical algorithms, which resulted in numerical instability and sometimes in poor convergence.

All of the mentioned models were developed and compared with experiments on hydrodynamic cavitation, where very rapid driving pressure changes are unlikely to occur. This is quite different in acoustic cavitation, where bubble growth and collapse are driven by ultrasound (>20kHz) and the driving pressure switches from positive to negative values periodically in a matter of microseconds. Additionally to the faster excitation pressure time scales, other essential differences occur for acoustically driven as compared to hydrodynamically driven cavitation: bubbles can show longer life time in terms of collapse cycles (up to hundreds), and they are re-circulated. Both leads, together with acoustic bubble-bubble interaction, to characteristic structure formation [19-21]. Furthermore, the bubble distribution acts back on the driving pressure wave by acoustic impedance change of the two phase medium - a phenomenon that typically does not play a role in hydrodynamic cavitation problems. For these reasons, the models for numerical simulation of acoustic cavitation are rather distinct from the hydrodynamic codes mentioned above. They traditionally split into "continuum models" and "particle models". The former focus on the acoustic wave propagation in bubbly (cavitating) liquids and couple the gas/vapour resp. bubble density, which is given by a continuous field variable in space and time, to the acoustic pressure amplitude [19, 22-26]. The latter resolve the bubble population into individual bubbles ("particles") and focus on their dynamics, motion and re-distribution driven by the sound wave and acoustic forces [27, 28]. Recently, also hybrid forms and combinations of the two model types have been proposed [29-31]. Nevertheless, the development of simulation codes of acoustic cavitation with sufficient predictive power is still ongoing; see e.g. [32].

Yet, the standard acoustic cavitation model approaches prove inefficient in cases were acoustic cavitation resembles the hydrodynamic one – with large coherent gas/vapour structures. Then the notion of "bubbly liquid" or individually acting bubbles in a cloud or streamer is not appropriate. Likewise, hydrodynamic models can fail to accurately reproduce acoustically driven cavitation due to the high frequency of the pressure fields. In the following we focus on a peculiar case which appears somehow intermediate between hydrodynamic and acoustic cavitation, namely a large cavity attached to an ultrasonic horn tip and collapsing with its self-generated subharmonic cycle frequency ("acoustic supercavitation"). Here we report that several standard hydrodynamic codes were not able to reproduce the experimental observations, but that a suitable extension of the vapour source term removes the deficiencies and leads to a convincing simulation result by the new code.

2 Problem Statement and Conventional Simulation

Ultrasonic horn transducers are frequently used in applications like ultrasonic homogenization, sonochemical reactions, milling, emulsification, spraying and cell disruption (the applications of acoustic cavitation go even further – for example water purification, surface cleaning and lithotripsy).

They are operated typically in the frequency range up to about 50 kHz and have tip diameters from some mm to several cm. It has been observed that if the horn tip is sufficiently small and driven at high amplitude, cavitation is very strong, and the tip can be covered entirely by the gas/vapour phase for longer time intervals. In Fig. 1 an acoustic horn emitter of small diameter (3 mm) and oscillation amplitude of 164 μm at 20 kHz is shown for several representative cycles. A large single cavity of a large extension occurs at the tip, while a cloud of individual bubbles is seen below. In this condition, the horn tip is working most of the time against gas and only in short intervals against liquid. The large attached cavity is undergoing a characteristic "mushroom" shape oscillation with strong collapse. It is generating its own oscillation frequency which is smaller than the driving and thus falls into the subharmonic range of the excitation frequency f_0 (for instance somewhere between $f_0/6$ to $f_0/4$). The subharmonic acoustic emission generated by the large bubble can be even more pronounced in an acoustic power spectrum than the primary wave [33].

It was suggested by the present authors [1] to term the observed phenomenon of attached cavities partly covering the full horn tip as “acoustic supercavitation”. This reflects the conjecture that not the sound field in terms of acoustic (negative) pressure in the bulk liquid is responsible for nucleation, but the rapid motion of the transducer surface.

As already mentioned, modeling of such a phenomenon by a “conventional” hydrodynamic cavitation model, which would be a reasonable choice of an approach, results in poor accuracy. As an example, in Fig. 2 modeling by the Schnerr-Sauer model [12] is shown. Other models [6, 9, 11] were tested with the similar result to fail in predicting the low frequency oscillation of the large attached cavity and its extent.

One can see that the Schnerr-Sauer model predicts a cavity of a significantly smaller size (compared to the one in Fig. 1), which additionally follows quite periodically the driving frequency of the horn (20 kHz, duration of a period is 50 μs). While indeed a cavity at the tip is reproduced, essentials like the cavity's (subharmonic) dynamics and its correct size are clearly missed.

In the next Section we first investigate the background in development of a cavitation model. Then, also based on our experimental observations (more thoroughly discussed in [1]), we build a new, more detailed model, which does not neglect the second derivatives in the Rayleigh-Plesset equation as previous models.
Finally, in Sec. 4 we employ the new model for the acoustic supercavitation problem. Comparisons reveal a good agreement with the measurements of the intense cavitating flow in the vicinity of the ultrasonic horn transducer tip.

3 Development of Cavitation Model

The most commonly used approach to the modeling of hydrodynamic cavitation employs the transport equation for the vapour phase with (semi-)empirically derived source terms for the description of vapour generation and destruction. There exist several variants with only slightly different relationships (Tab 1).
One needs to bare in mind that the constants included in the models (C_{dest} and C_{prod}) are not necessarily the same and were fine tuned for each model on specific experimental results. All models presented in Tab. 1 use some kind of pressure dependent source terms to describe the evaporation and condensation processes. For the cases where the Weber umber is low (in the present case We ≈ 0.01) it is only logical to use a part of the Rayleigh-Plesset equation for this purpose as it is physically related to the spherical bubble dynamics and it was proven many times to be an effective way of modeling cavitation. The

terms with the square root in Tab. 1 stem from an approximate solution for bubble expansion or collapse:

$$S \propto \frac{dR}{dt} = \pm\sqrt{\frac{2}{3}\frac{|p_v(T_\infty) - p_\infty|}{\rho_l}} \tag{1}$$

This "Rayleigh solution" (Eqn. 1) is obtained by neglecting several terms of the general Rayleigh-Plesset equation (the term is considered positive (+) for evaporation when the ambient pressure p_∞ is lower than the vapour pressure p_v and negative (-) in the case of condensation). Based on our observations [1] we concluded that it is probably this oversimplification that leads to the poor prediction of the dynamics of the cavitation at the ultrasonic horn by the present models [6, 9, 11, 12]. The main task is therefore the determination of the terms in the Rayleigh-Plesset equation, which cannot be neglected if one wants to correctly predict the cavitation dynamics in a rapidly changing pressure field.
It seems that Kanfoudi at al. [34] already approached this idea, however they did not consider the possibility of applying it to rapidly changing pressure fields and had to significantly alter the model constants to obtain agreement with experimental results. This points to another possible reason for poor performance of the existing models (Tab. 1) – they all consider a relatively large scale of the cavity whereas we are dealing with small scale vapour structures. As mentioned in [35] this could result in issues of dynamic similarity and scale effects by the model constants – however for the present case this is unlikely as our sensitivity study showed marginal influence of the model constants values.

3.1 The Schnerr - Sauer model

Based on our positive previous experience and experimental data (shown later in Sec. 3.2.1) we decided to build a new code on the foundations of the Schnerr-Sauer model [12] which utilizes the homogenous mixture approach to model cavitation – of course one could apply the presented approach also to any other model from the family above. A transport equation for vapour volume fraction is solved in order to determine the density of the liquid-vapour mixture:

$$\frac{\partial(\rho_v \alpha)}{\partial t} + \nabla \cdot (\rho_v \alpha u) = S_{prod.} + S_{dest.} = S \tag{2}$$

where S represents the source term, which describes creation or destruction of vapour. A relatively straightforward derivation [12] leads to the formulation of the already given source term:

$$S = \pm\frac{\rho_l \rho_v}{\rho_m}\frac{3\alpha(1-\alpha)}{R}\frac{dR}{dt} \tag{3}$$

where *dR/dt* denotes the velocity of a spherical bubble surface, representing bubble growth. At this point cavitation models [9-12] utilize the Rayleigh solution (Eqn. 1). As already mentioned this is not appropriate in the case of rapidly changing pressure fields, and hence we propose to replace it with the equation of bubble growth velocity based on the simplified Rayleigh-Plesset equation derived in the following section.

3.2 Simplyfing the Rayleigh - Plesset equation

The general Rayleigh-Plesset equation can be written as [2]:

$$\underbrace{\frac{p_v(T_\infty)-p_\infty}{\rho_l}}_{1}+\underbrace{\frac{p_v(T_b)-p_v(T_\infty)}{\rho_l}}_{2}+\underbrace{\frac{p_{g0}}{\rho_l}\left(\frac{R_0}{R}\right)^{3\gamma}}_{3}=\underbrace{R\frac{d^2R}{dt^2}}_{4}+\underbrace{\frac{3}{2}\left(\frac{dR}{dt}\right)^2}_{5}+\underbrace{\frac{2\sigma}{\rho_l R}}_{6}-\underbrace{\frac{4\mu}{\rho_l R}\frac{dR}{dt}}_{7} \quad (4)$$

Here the first term represents the pressure difference between the vaporization pressure at T_∞ and the pressure in the vicinity of the bubble. The second and third terms describe the influence of the temperature and gases inside the bubble. The inertial effects are given by the fourth and the fifth term, while terms 6 and 7 depict the influence of surface tension and liquid viscosity, respectively.

As one can see, the Rayleigh solution (Eqn. 1) of the given equation follows the neglect of all terms except the first one and the velocity part of the inertial term (term 5 in Eqn. 4). This is appropriate when one has to deal with hydrodynamic cavitation at "usual" flow conditions (water as liquid at approximately 20°C), as the thermal, gaseous, surface tension and viscous influences are negligible compared to the pressure difference [36]. Further on, the acceleration term can also be neglected as the typical time discretization scale in such simulations is relatively long, and the acceleration to the asymptotic velocity of the bubble growth takes only a short period of time. This is typically shorter than 10^{-4} s and decreases with the increase of the pressure difference between bubble inner and surrounding pressure [36]. Although the same cannot be said in the case of bubble collapse, the Rayleigh solution provides satisfactory approximation for this period of bubble dynamics in hydrodynamic cavitation as well [36].

To determine which terms cannot be neglected in our particular case (or in a general case with steep pressure gradients), different aspects need to be considered. Firstly, as this cavitation has both acoustic and hydrodynamic characteristics (cavitation is driven by acoustical waves, but resembles hydrodynamic cavitating flow [1]), the influence of liquid and gaseous variables have to be reassessed. This was done experimentally. Only the main results and conclusions of the experimental campaign are given in the present manuscript – for a more detailed description of the experimental work and an extensive discussion on the physics of the cavitating flow near the small ultrasonic horn we refer to [1].

3.2.1 Experiments

The cavitation was produced by an ultrasonic horn transducer (Bandelin HD 2070) with a tip diameter of 3 mm, which was submerged vertically into a 125 ml glass cuvette. The horn was submerged 1 cm deep into the water, 3 cm from the bottom of the cell.
A high-speed camera (Photron FASTCAM SA5 model 1000K-M1) was used for observation of cavitation from the side at 100000 frames per second, and simultaneously the acoustic pressure was measured by a hydrophone (Reson TC4038, 3 mm diameter).

We investigated how the attached cavitation changes when the ultrasonic horn operates at different powers. For a much more thorough description of the study one should refer to [1]. If the power density was sufficient (above 280 W/cm^2), similar conclusions could be drawn for all cases. Hence, only results at 70 W power (990 W/cm^2 power density), 164 µm oscillation amplitude at 20 kHz, are shown (comparison between experimental results at 30 and 50W and simulations are given in Fig. 9). The main goal of this part of the study is to investigate the fluid parameters, which could influence or explain the peculiar (slow) dynamics of cavitation on the small ultrasonic horn. We tested the influence of:

- Presence of gas in the liquid. Degassing the water could reduce or suppress bubble nucleation.
- Viscosity. It could influence the intensity of the turbulence and consequently also cavitation inception, as the pressure can locally drop below vapour pressure inside the eddies.

Furthermore, damping of the sound wave and the bubble oscillation is increased with viscosity.

- Surface tension. It could influence the critical amplitude of acoustic pressure at which cavitation nuclei begin to rapidly grow into bubbles.
- Temperature. The increase of temperature leads to increase of vapour pressure and by this to the conditions more prone to cavitation. There will also be indirect changes of viscosity, surface tension and density due to the variation of the temperature (the experiments were conducted in a way to minimize these, indirect, effects).

The main results of the experimental campaign are shown in Fig. 3, which presents the attached cavity size and pressure evolutions in time for different fluid parameters, and in Tab. 2 where the maximum size of the attached cavitation and its mean oscillation frequencies are listed according to fluid parameters.

As can be deducted from Fig. 3 and Tab. 2, both the typical attached cavity oscillation frequency and the maximum volume of the cavity are almost unaffected by the fluid parameters. From the diagrams in Fig. 3 one can see that the evolution of the cavitation volume changes only slightly, with more obvious changes in the evolutions of the pressure. This is probably related to different attenuation of the signal [1].
One can conclude, on the basis of these experiments, that terms 2, 3, 6 and 7 in the Rayleigh – Plesset equation (Eqn. 4) can be neglected in the new cavitation model, namely temperature, (non-condensable) gas pressure, surface tension, and viscosity. The only relevant additional part appears to be the second derivative (4) representing the inertial terms.

Its relevance also becomes clear if we remember that the driving frequency of the horn (in the present case) lies at 20 kHz. From a numerical point of view this means that the time step has to be considerably shorter than 10^{-5} s. As a consequence the acceleration (term 4) cannot be disregarded, as the bubble will still be accelerating its growth velocity during such a short time interval (it takes 10^{-4} s or less to reach a stationary growth) [36].

With the before mentioned considerations, we obtain the simplified Rayleigh-Plesset equation, which can be used to obtain the source term of the new model:

$$\frac{p_v(T_\infty) - p_\infty}{\rho_l} = R\frac{d^2R}{dt^2} + \frac{3}{2}\left(\frac{dR}{dt}\right)^2 \tag{5}$$

3.3 Final form of the cavitation model

As the source term equation includes an acceleration term d^2R/dt^2, the derivation of the velocity dR/dt (in Eqn. 5) is not straightforward as in other existing models [9-12]. Here we split the calculation of the velocity dR/dt into two parts. First we determine the acceleration:

$$\frac{d^2R}{dt^2} = \frac{p_v(T_\infty) - p_\infty}{\rho_l R} - \frac{3}{2R}\left(\frac{dR}{dt}\right)^2 \tag{6}$$

After this, the velocity of bubble growth can be calculated for each iteration within a time step in a finite difference scheme as:

$$\frac{dR}{dt}(t) = \frac{dR}{dt}(t - \Delta t) + \frac{d^2R}{dt^2}(t)\Delta t \tag{7}$$

We calculate the bubble growth velocity at the end of a time step and then use it as a "base" velocity to which the acceleration term is added during iterations in the next time step. 8. The initial conditions for both derivatives (*dR/dt* and d^2R/dt^2) were set to 0.

Simulations proved to be unstable since negative volume fractions of vapor could occur during the collapse phase. Hence an additional stability criterion had to be derived and implemented.

3.3.1 Stability criterion

The collapse velocity increases rapidly as the volume fraction approaches the zero value [36, 37]. Consequently the cavitation source term (Eqn. 3) would grow to a value, which would change the vapour volume fraction α to an unphysical (negative) value. To avoid this possibility a stability criterion was introduced. At the very end of the bubble collapse the time derivative term in the transport equation for volume fraction α (Eqn. 3) is much larger than its convective term. Hence we can neglect the former one and obtain

$$\frac{\partial(\rho_v \alpha)}{\partial t} \approx S \tag{8}$$

Knowing that the minimum value of vapor volume fraction is 0, one can write this equation in discrete manner and obtain the maximum allowed collapse velocity for a certain given time step Δt:

$$\left(\frac{dR}{dt}\right)^t_{\max} = -\frac{\rho_v(t-\Delta t)\alpha(t-\Delta t)}{\Delta t}\frac{\rho_m(t)R(t)}{\rho_v(t)\rho_l(t)3\alpha(t-\Delta t)(1-\alpha(t-\Delta t))} \tag{9}$$

This velocity is determined at the end of each time step and is used as limiting condition in the calculation of the velocity in the next time step – in case of a bubble collapse, if the *dR/dt* from the model (Eqn. 7) exceeds the value of the *dR/dt* from Eqn. 9 the latter is used.

3.4 Model constants

Like the original model [36], the present approach requires the input of nuclei number density n_0 and the initial nuclei size R_0 - the two values define the initial local vapour volume fraction in Eqn. 3. According to the recommendations in [12, 38, 39] n_0 was set to $n_0 = 10^{12}$ 1/m^3. The size of the nuclei could be determined from close inspection of images just prior to the cavity growth (for example the first frame in Fig. 1) – it was set to $R_0 = 25$ μm. Predictions of simulations proved immune against reasonable variation of the n_0 and R_0 values.

4 Numerical simulation

The commercial program package Ansys Fluent was used to perform the simulations. The numerical model uses an implicit finite volume scheme. Due to higher robustness and better convergence a coupled velocity-pressure coupling scheme was used. Second order upwind differentiating schemes were used in spatial discretization of momentum and turbulent kinetic energy equations. The Green-Gauss Node Based method [39] was used for gradient discretization. For the interpolation of the pressure, the PRESTO! method [40] was employed. For the sake of higher stability a first order upwind discretization was chosen for calculation of the continuity and vapour volume fraction transport

equations. Because both phases were treated as compressible, the energy equation was used and discretized with a second order upwind method. For temporal discretization, a first order implicit formulation was used.

4.1 Geometry and mesh

Because the walls of the rectangular cuvette are relatively far from the cylindrically shaped horn tip, the problem can be simplified to a fully axisymmetrical case with negligible error. The computational domain extended over one half of the (now cylindrical) cuvette with the dimensions of 50 mm height and 25 mm radius, in which the horn tip of 3 mm diameter is placed vertically from top 30 mm above the bottom (compare Fig. 4).

All the boundary conditions were Dirichlet type. For the walls of the couvette and the horn we used the no-slip boundary condition for velocity. The top of the couvette was defined as the pressure outlet (gauge pressure 0 Pa).

The simulated horn oscillated in a sinusoidal manner at a frequency of 20 kHz, at various amplitudes, depending on the power. To capture the movement a dynamic mesh approach was used – the mesh must constantly (at each time step) be updated by smoothing and local remeshing [41].

Three mesh densities were tested and it was found that it does not influence the outcome of the calculation of cavitation dynamics. To check the influence of spatial discretization, a study of the discretization error on the basis of the Richardson extrapolation [42] was made and an error of 0.9 % was estimated. Results presented in the next section were calculated on a medium coarse mesh with 9800 cells (Fig 4).

It was determined that the mesh, due to very small deformation of the domain, preserves an extremely low value of cell equiangle skew.

4.2 Equations of the flow

To close the system of equations the software solved time dependent Reynolds-Averaged continuity equation, momentum equations, vapor volume fraction transport equation, the equations of the turbulence model and, since both phases were treated as compressible, the energy equation (to consider the compressibility of the liquid water the Tait equation of state [2] was used). As mentioned, a dynamic mesh approach was used to take into account the sinusoidal movement of the horn. The set of equations was therefore modified to consider the difference between the fluid and grid velocity. The integral form of the conservation equation for a general scalar ϕ (specific mass (unity) for continuity equation, specific momentum (velocity) for momentum equation, volume fraction for volume fraction equation and specific energy for the energy equation) on an arbitrary control volume, V whose boundary is moving can be written as:

$$\frac{d}{dt}\int_V \rho\phi dV + \int_A \rho\phi\left(\vec{u}-\vec{u}_g\right)\cdot d\vec{A} = \int_A \Gamma\nabla\phi\cdot d\vec{A} + \int_V S_\phi dV \,, \tag{10}$$

where ρ is the fluid density, $\vec{u}$ is the flow velocity vector, $\vec{u}_g$ is the grid velocity of the moving mesh, Γ is the diffusion coefficient and S_ϕ is the source term of ϕ. A is used to represent the boundary of the control volume V.

The equations were combined with the newly developed cavitation model, described in the previous section. In addition, also equations of state, which describe the relation between the pressure and the

liquid and vapor densities and the relations for the volume fraction and the mixture (liquid-vapour) density and viscosity, had to be introduced.
The flow in the vicinity of the horn is clearly turbulent (the Reynolds number based on the horn diameter and maximal flow velocity lies in the range of 15000), hence a k-ε realizable model [43] was used, as it offers better accuracy in areas, which are specific for the flow around an ultrasonic horn (development of cylindrical jets, boundary layers under the influence of adverse pressure gradient, flow detachment and recirculation). The boundary layer influence on flow development was considered with the use of enhanced wall functions [44].

4.3 Convergence criteria
The criterion for a converged time step solution was determined by observation of the static pressure at a point 7 mm horizontally from the tip of the horn (position of the hydrophone in the experiments). The value of static pressure always converged when the residuals decreased by 3 orders of the magnitude. Finally we have chosen a convergence criterion of 10^{-4} (10^{-8} for the energy equation) to minimize the iteration error, which was estimated to 0.1% [42]. Approximately 40 iterations per time step were needed to obtain a converged time step solution.

5 Results
Simulations with the new cavitation model were compared with experiments – namely the evolution of the volume of vapour structures, their topology, the pressure evolution and the mean velocity field in the vicinity of the horn tip were considered. In the first part (Figs. 5-8) results for the test A (Tab. 2) are graphically presented and commented. Since the physics of the flow and the results do not differ significantly between the cases, the results of other tests (B-E in Tab. 2 and additionally for two different ultrasonic horn powers – 30 and 50W) are given more briefly in Fig. 9.

Figure 5 shows the prediction of the cavitation structure beneath the tip of the horn. The instants shown correspond to the ones in Fig. 1.

As in the experiment (Fig. 1) the cavity firstly grows and forms a characteristic “mushroom” shape (between 40 and 80 μs). The maximum volume is achieved about 100 μs after the start of the growth. The cavity then contracts at the outer rim, while its axial size remains almost constant for another 50 μs. The main cavity collapse occurs roughly 180 μs after the start of the cycle. A brief rebound follows, where a toroidally shaped cloud forms for about 20 μs (probably due to a strong toroidal vortex beneath the tip). During each cavitation period (about 200 μs or 5 kHz) the tip of the horn advances and retracts about 4 times (at 20 kHz). The same periodicity and the dynamics could also be observed during the experiments.

A comparison between the measured and predicted cavity volume is given in Fig. 6.

It is evident that the simulation accurately predicts the dynamics of the cavity volume. Some discrepancies do exist though – possibly due to the inability of the simulation to capture the single small bubble jetting (seen in Fig. 1) when the cavity is the largest (the volume of the single bubbles are considered in experiment but not in simulation). One can also observe a rebound of the cavity just before the end of the second period in Fig. 6.

The small oscillations superimposed to the main volume oscillations, well visible during the time when the size of the cavity is close to its maximum, can be attributed to the movement of the tip of the horn, as their period of 50μs corresponds to the 20 kHz driving frequency. Their amplitude of approximately

1mm^3 is roughly equal to the moving volume of the horn ($V = h \cdot \pi r^2 = 164\mu m \cdot \pi \cdot (1.5mm)^2 = 1.15mm^3$). In the experimental curve this moving volume does not appear as it could not be resolved from the images.

The measured and predicted pressure evolutions at the position indicated below and during the same time frame are shown in Fig. 7.

At every cavity collapse a pressure wave is emitted and recorded by a hydrophone (or a monitor in the simulation) positioned at a distance of 7 mm from the tip of the horn. It reaches a peak amplitude of about 4 bar, and peak negative amplitude of -1 bar. It is evident that the frequency of the pressure peaks is correctly predicted. The peak pressure amplitude seems to be slightly overpredicted. This could be a result of the choice of the water compressibility model and the fact that in the simulation we are not considering the influence of inclusion of small single bubbles on attenuation of the pressure wave (these can be nicely seen in Fig. 1). Furthermore, contributions of non-condensable gas in the cavity - not considered in the simulations - might damp the acoustic emissions during its collapse.

Finally also the mean measured and predicted velocity fields were compared (Fig. 8). For the case of the measured profile a method based on the advection diffusion equation [45, 46], which couples the velocity field with the field of concentrations of a passive tracer (in the present case cavitation bubbles), was used. One needs to bear in mind that the measurement gives the velocity of the vapour phase while the simulation considers a velocity in a mixed fluid – these can differ significantly [47].

The periodical movement of the horn creates a flow away from the tip (downwards) near the axis of the horn. As the flow looses momentum it turns radially outwards, and then upwards. One can observe a significant toroidal vortex which forms beneath the outer rim of the tip of the horn. We believe that it is this vortex that initiates the rebound of the cavity at the end of its period (Fig. 5, frame at 180 μs). The velocity fields (measured (left) and predicted (right)) qualitatively agree reasonably. The very clear vorticity shown in the simulation is less pronounced in the experimental results – it can be seen a bit closer to the face of the horn but somewhat further away from its center. The qualitative and quantitative deviations probably origin from the different velocities of vapour (experiment) and liquid/vapour mixture (simulation).

In Fig. 9 we present comparisons of measured and predicted values of characteristic attached cavitation bubble oscillation frequency, its maximal volume and the maximal recorded pressure for all cases (A-E in Tab. 2 and additional two for the same fluid properties as in test A but at a reduced power – 30 W (test F) and 50 W (test G)).

When one compares the quantitative agreement between the measurements and simulations (Fig. 9) an obvious improvement can be seen when the new cavitation model is employed. Results obtained with existing models (results obtained by the original Schnerr – Sauer model [12] are shown for comparison in Fig. 9) poorly predict the characteristic parameters of cavitation in our case. Without the acceleration term, the existing model is unable to predict the slow cavitation dynamics – the cavity always follows the driving frequency (20 kHz). As a consequence the attached cavity does not grow to its correct size (its maximal size is in average 30 % too small compared to the experiment) and implodes at a significantly lower aggressiveness (about 1 bar pressure wave instead of 4 bar was continuously predicted).
With the new model the values significantly improve. The characteristic cavitation frequency is very accurately predicted – the average discrepancy lies at only 1 %. The maximal cavitation volume is

predicted at somewhat worse accuracy (within 5 %). Finally about 7 % prediction accuracy was achieved for the maximal recorded pressure at 7 mm distance from the tip of the horn.

6 Conclusions

In our study we were concerned with the numerical simulation of a peculiar type of attached cavitation at an ultrasonic horn transducer tip ("acoustic supercavitation" [1]). We first evaluated several existing hydrodynamic cavitation models [9-12]. All of them have proven to be unable to correctly predict the main features of the cavitating flow in the vicinity of the horn tip – namely the attached cavity oscillation frequency, cavity size and pressure pulsations.

It is common for many models to build the evaporation and condensation source terms around a much simplified Rayleigh – Plesset equation. Based on experiments, which are more thoroughly discussed in [1] and estimations of the time scales (the length of the transition to the asymptotic bubble wall velocity is not negligible compared to the numerical time step [12]), we concluded that the most commonly used simplification is too rough for cases with rapid pressure dynamics and that one should also include the second derivative term of the Rayleigh-Plesset equation (Eqn. 4) in the cavitation model. We tested the newly developed model against measurements on ultrasonic horn cavitation and obtained accurate results in terms of cavitation dynamics, cavity volume, pressure pulsations and velocity fields.

The new model seems particularly suited for simulations of cavitating flows where the dynamics of pressure fluctuations is high – apart from ultrasonic horns, for example: ultrasonic baths, rapid pump startup [48] and in pumps operating under the POGO phenomenon [49]. Further work will show if this approach results in improved results in the other cases as well.

Acknowledgments

We thank Viet Anh Truong from Hanoi University of Science and Technology for valuable discussions and Carlos Cairós for extensive help with experimental part of the work. Many thanks go to Jörg Enderlein and Qi Van from Drittes Physikalisches Institut, Göttingen University, for loan of equipment. The financial support by the Austrian Federal Ministry of Economy, Family and Youth and the Austrian National Foundation for Research, Technology and Development, Lam Research AG (Austria) and European Space Agency is gratefully acknowledged.

References

[1] Žnidarčič A, Mettin R, Cairós C, Dular M. Attached cavitation at a small diameter ultrasonic horn tip. Physics of fluids, 2014; 26 (2): 1-17.

[2] Franc J P, Michel J M. Fundamentals of Cavitation, Kluwer Academic Publishers, 2004.

[3] Alajbegovic A, Groger H A, Philipp H. Calculation of transient cavitation in nozzle using the two-fluid model. 12th Annual Conference on Liquid Atomization and Spray Systems, Indianapolis, IN, USA, 1999.

[4] Kubota A, Hiroharu K, Yamaguchi H. A new modelling of cavitating flows, a numerical study of unsteady cavitation on a hydrofoil section. J. Fluid Mech. 1992; 240: 59–96.

[5] Kunz R, Boger D, Chyczewski T, Stinebring D, Gibeling H. Multi-phase CFD analysis of natural and ventilated cavitation about submerged bodies. ASME FEDSM99-7364, SAN Francisco, 1999.

[6] Merkle C L, Feng J, Buelow P E O. Computational modeling of the dynamics of sheet cavitation. 3rd Int. Symp. on Cavitation, Grenoble, France, 1998.

[7] Owis F M, Nayfeh A H. Numerical simulation of 3-D incompressible, multi-phase flows over cavitating projectiles. Eur. J. Mech. B Fluids 2004; 24: 339–351.

[8] Senocak I, Shvy I W. A pressure-based method for turbulent cavitating flow simulations. J. Comput. Phys. 2002; 176: 363–383.

[9] Singhal A K, Li H, Atahavale M M, Jiang Y. Mathematical basis and validation of the full cavitation model. J. Fluids Eng. 2002; 124: 617–624 .

[10] Frobenius M, Schilling R, Bachert R, Stoffel B. Three-dimensional, unsteady cavitation effects on a single hydrofoil and in a radial pump – measurements and numerical simulations, Part two: Numerical simulation. Fifth International Symposium on Cavitation, Osaka, Japan, 2003 .

[11] Zwart P J, Gerber A G, Belamri T. A Two-Phase Flow Model for Predicting Cavitation Dynamics. Fifth International Conference on Multiphase Flow, Yokohama, Japan, 2004.

[12] Schnerr G H, Sauer J. Physical and numerical modelling of unsteady cavitation dynamics. 4th International Conference on Multyphase Flow, ICMF-2001,New Orleans, USA, 2001.

[13] Dauby D, Queutey P, Leroyer A, Visonneau M. Computation of 2D cavitating flows and tip vortex flows with an unstructured RANSE solver. 11èmes journées de l'hydrodynamique Brest, 3-5 avril, 2007.

[14] Delannoy Y, Kueny J L. Two phase flow approach in unsteady cavitation modelling. Cavitation and Multiphase Flow Forum, ASME- FED 1990, 153–158.

[15] Coutier-Delgosha O, Fortes-Patella R, Reboud J L. Evaluation of turbulence model influence on the numerical simulations on unsteady cavitation. J. Fluids Eng. 2003; 125: 38–45.

[16] Hofmann M, Lohrberg H, Ludwig G, Stoffel B, Reboud J L, Fortes-Patella R. Numerical and experimental investigations on the self – oscillating behaviour of cloud cavitation – Part 1: Visualisation. 3rd ASME/JSME Joint Fluids Engineering Conference, San Francisco, CA, 1999.

[17] Lohrberg H, Stoffel B, Fortes-Patella R, Reboud J L. Numerical and experimental investigations on the cavitation flow in cascade of hydrofoils. Exp. Fluids 2002; 33: 578–586.

[18] Song C C S, He J. Numerical simulation of cavitating flows by single-phase flow approach. 3rd International Symposium on Cavitation, Grenoble, France, 1998, 295–300.

[19] Akhatov I, Parlitz U, Lauterborn W. Pattern formation in acoustic cavitation. J. Acoust. Soc. Am. 1994; 96: 3627-3635.

[20] Parlitz U, Mettin R, Luther S, Akhatov I, Voss M, Lauterborn W. Spatio–temporal dynamics of acoustic cavitation bubble clouds. Phil. Trans. R. Soc. Lond. A 1999; 357: 313-334.

[21] Mettin R. Bubble structures in acoustic cavitation. In: Doinikov A A (ed.): Bubble and Particle Dynamics in Acoustic Fields: Modern Trends and Applications, Research Signpost, Kerala (India) 2005: 1-36.

[22] Van Wijngaarden L. On the equations of motion for mixtures of liquid and gas bubbles. J. Fluid Mech. 1968; 33: 465-474.

[23] Caflisch R E, Miksis M J, Papanicolaou G C, Ting L. Effective equations for wave propagation in bubbly liquids. J. Fluid Mech. 1985; 153: 259-273.

[24] Karpov S, Prosperetti A, Ostrovsky L. Nonlinear wave interactions in bubble layers. J. Acoust. Soc. Am. 2003; 1132: 1304-1316.

[25] Dähnke S, Keil F J. Modeling of three-dimensional linear pressure fields in sonochemical reactors with homogeneous and inhomogeneous density distributions of cavitation bubbles. Industrial & engineering chemistry research 1998; 37(3): 848-864.

[26] Servant , Hita A, Caltagirone J P, Gérard A. On the interaction between ultrasound waves and bubble clouds in mono- and dual-frequency sonoreactors. Ultrason. Sonochem. 2003; 10: 347-355.

[27] Mettin R, Luther S, Ohl C D, Lauterborn W. Acoustic cavitation structures and simulations by a particle model. Ultrason. Sonochem. 1999; 6: 25-29.

[28] Mettin R. From a single bubble to bubble structures in acoustic cavitation. In: Kurz T, Parlitz U, Kaatze U (eds.): Oscillations, Waves and Interactions, Universitätsverlag Göttingen, Göttingen 2007: 171-198.

[29] Mettin R, Koch P, Lauterborn W, Krefting D. Modeling acoustic cavitation with bubble redistribution. In: Sixth International Symposium on Cavitation 2006: 75 (1-5).

[30] Louisnard O. A simple model of ultrasound propagation in a cavitating liquid. Part I: Theory, nonlinear attenuation and traveling wave generation. Ultrason. Sonochem. 2012; 19: 56-65.

[31] Louisnard O. A simple model of ultrasound propagation in a cavitating liquid. Part II: Primary Bjerknes force and bubble structures. Ultrason. Sonochem. 2012; 19: 66-76.

[32] Jamshidi R, Brenner G. Dissipation of ultrasonic wave propagation in bubbly liquids considering the effect of compressibility to the first order of acoustical Mach number. Ultrasonics 2013; 53: 842-848.

[33] Truong V A. A Study of Impulsive Pressure Distribution of Cavitation Generated by a High Frequency Vibrational Probe. J. of Science and Technology 2009; 73, Technical Universities Pub.

[34] Kanfoudi H, Lamloumi H, Zgolli R. A new model to simulate a cavitating flow. International Renewable Energy Congress, IREC 2010, November 5-7, 2010.

[35] Martynov S B, Mason D J, Heikal M R. Numerical simulation of cavitation flows based on their hydrodynamic similarity. Int. J. Engine Res. 2005; 7(3): 283-296.

[36] Sauer J. Instationaer kavitierende Stroemungen – Ein neues Modell, basirend auf Front Capturing (VoF) und Blasendynamik. PhD thesis, Universitaet Karlsruhe, Karlsruhe 2000.

[37] Frobenius M. Numerische Simulation kavitierender Stroemungen in hydraulischen Stroemungsmaschinen. PhD thesis, Technische Universitaet Muenchen, Muenchen 2004.

[38] Young F R. Cavitation. Mc Graw-Hill Book Company, London, 1999.

[39] Holmes D G, Connell S D. Solution of the 2D Navier-Stokes Equations on Unstructured Adaptive Grids. AIAA 9th Computational Fluid Dynamics Conference, June, 1989.

[40] Patankar S V. Numerical Heat Transfer and Fluid Flow. Hemisphere, Washington, DC, 1980.

[41] Batina J T. Unsteady Euler airfoil solutions using unstructured dynamic meshes. AIAA Journal 1990; 28(8): 1381–1388.

[42] Ferziger J H, Perić M. Computational Methods for Fluid Dynamics. 2nd ed. 1999; Springer Verlag.

[43] Shih T H, Liou W W, Shabbir A, Yang Z, Zhu J. A New k-e Eddy-Viscosity Model for High Reynolds Number Turbulent Flows - Model Development and Validation. Computers Fluids 1995; 24(3): 227-238.

[44] Kader B. Temperature and Concentration Profiles in Fully Turbulent Boundary Layers. Int. J. Heat Mass Transfer 1981; 24(9): 1541-1544.

[45] Bajcar T, Širok B, Eberlinc M. Quantification of flow kinematics using computer-aided visualization. J. Mech. Eng. 2009; 55 (4): 215-223.

[46] Web page www.admflow.net

[47] Khlifa I, Coutier-Delgosha O, Hocevar M, Fuzier S, Vabre A, Fezzaa K, Lee W K. Fast X-Ray Imaging for Velocity Measurements in Cavitating Flows. 8th international Symposium on Cavitation, CAV 2012, Singapore 2012, doi:10.3850/978-981-07-2826-7_295.

[48] Duplaa S, Coutier Delgosha O, Dazin A, Bois G. X-Ray Measurements in a Cavitating Centrifugal Pump During Fast Start-Ups. Journal of Fluids Engineering 2013; 135 (4): 041204.

[49] Rubin S. Longitudinal instability of liquid rockets due to propulsion feedback (Pogo). J. Spacecraft and Rockets 1966; 3(8): 1188–1195.

Figure captions

Fig. 1: Two cycles of the oscillation of a large cavity at an ultrasonic horn tip of 3 mm diameter in water (acoustic frequency 20 kHz, recording at 100000 frames/s (only every 2nd image is shown), exposure 1 µs, sequence row by row from top left). Conditions are the same as for the case A in Tab. 1.

Fig. 2:Simulation of cavitation on an ultrasonic horn by the original Schnerr-Sauer model [12]. The boundary conditions correspond to the sequence shown in Fig. 1.

Fig. 3: Evolution of the size of attached cavitation and pressure for different fluid parameters.

Fig. 4: Computational domain.

Fig. 5: Sequence showing a simulation of cavitation on an ultrasonic horn with the new cavitation model for 164 µm horn oscillation amplitude at a frequency of 20 kHz (test A from Tab. 2).

Fig. 6: Comparison between the predicted and measured attached cavity volumes for 164 µm horn oscillation amplitude at a frequency of 20 kHz (case A from Tab. 2).

Fig. 7: Comparison between the predicted and measured pressure for 164 µm horn oscillation amplitude at a frequency of 20 kHz (case A from Tab. 2).

Fig. 8: Time averaged experimental (left) and predicted (right) velocity profiles in the vicinity of the tip of the horn for 164 µm horn oscillation amplitude at a frequency of 20 kHz (case A from Tab. 2)..

Fig. 9: Measured and predicted characteristic values of attached cavitation bubble oscillation frequency, maximal volume of the cavity and maximal recorded pressure for cases A-E (Tab. 2) and at 30 W (F) and 50W (G) power. The "original" model is Schnerr-Sauer from [12].

Table captions

Tab. 1: Source terms of some commonly used cavitation models.

Tab. 2: Maximum size of the attached cavitation structure and cavitation oscillation frequency for different fluid parameters.

Authors	Source terms
Kunz et al. [5]	$S_{prod.} = \frac{2C_{prod.}\rho_l \min\{0, p_\infty - p_v\}}{\rho_l u_\infty^2 t_\infty}$ $S_{dest.} = -\frac{C_{dest.}\rho_v \alpha_l^2 (1-\alpha_l)}{t_\infty}$
Merkle [6]	$S_{prod.} = \frac{2C_{prod.}\rho_l \min\{0, p_\infty - p_v\}\alpha_l}{\rho_v \rho_l u_\infty^2 t_\infty}$ $S_{dest.} = -\frac{2C_{prod.} \max\{0, p_\infty - p_v\}(1-\alpha_l)}{\rho_l u_\infty^2 t_\infty}$
Singhal et al. [9]	$S_{prod.} = C_{prod.}\frac{\sqrt{k}}{\sigma}\rho_l\rho_v\sqrt{\frac{2}{3}\frac{\lvert p_\infty - p\rvert}{\rho_l}}(1-f_v-f_g)$ $S_{dest.} = -C_{dest.}\frac{\sqrt{k}}{\sigma}\rho_l\rho_l\sqrt{\frac{2}{3}\frac{\lvert p_\infty - p\rvert}{\rho_l}}f_v$
Frobenious et al. [10]	$S_{prod.} = C_{prod.}\frac{n_0}{1+4/3n_0\pi R^3}4\pi R^2\sqrt{\frac{2}{3}\frac{\lvert p_\infty - p_v\rvert}{\rho_l}}$ $S_{dest.} = -C_{dest.}\frac{n_0}{1+4/3n_0\pi R^3}4\pi R^2\sqrt{\frac{2}{3}\frac{\lvert p_\infty - p_v\rvert}{\rho_l}}$
Zwart et al. [11]	$S_{prod.} = C_{prod.}\frac{3\alpha_{nuc.}(1-\alpha_v)\rho_v}{R}\sqrt{\frac{2}{3}\frac{\lvert p_\infty - p_v\rvert}{\rho_l}}$ $S_{dest.} = -C_{dest.}\frac{3\alpha_{nuc.}\alpha_v\rho_v}{R}\sqrt{\frac{2}{3}\frac{\lvert p_\infty - p_v\rvert}{\rho_l}}$
Schnerr and Sauer [12]	$S_{prod.} = \frac{\rho_l\rho_v}{\rho_m}\frac{3\alpha(1-\alpha)}{R}\sqrt{\frac{2}{3}\frac{\lvert p_\infty - p\rvert}{\rho_l}}$ $S_{prod.} = -\frac{\rho_l\rho_v}{\rho_m}\frac{3\alpha(1-\alpha)}{R}\sqrt{\frac{2}{3}\frac{\lvert p_\infty - p\rvert}{\rho_l}}$
Dauby et al. [13]	$S_{prod.} = C_{prod.}\rho_l \min\{0, p_\infty - p_v\}\alpha_l$ $S_{dest.} = -C_{dest.} \max\{0, p_\infty - p_v\}(1-\alpha_l)$

Case	Fluid	Temp.	Saturation	Viscosity	Surf. ten.	Mean freq.	Max. vol.
		°C	%	Pas	N/m	Hz	mm^3
A	H_2O	23	100	0.00093	0.072	5058	8.97
B	H_2O	23	50	0.00093	0.072	5085	8.58
C	H_2O+SDS	23	100	0.00093	0.05	5095	8.95
D	$C_2H_6O_2$	23	100	0.0169	0.048	5074	8.63
E	H_2O	45	100	0.0006	0.069	5074	8.87

Figure01

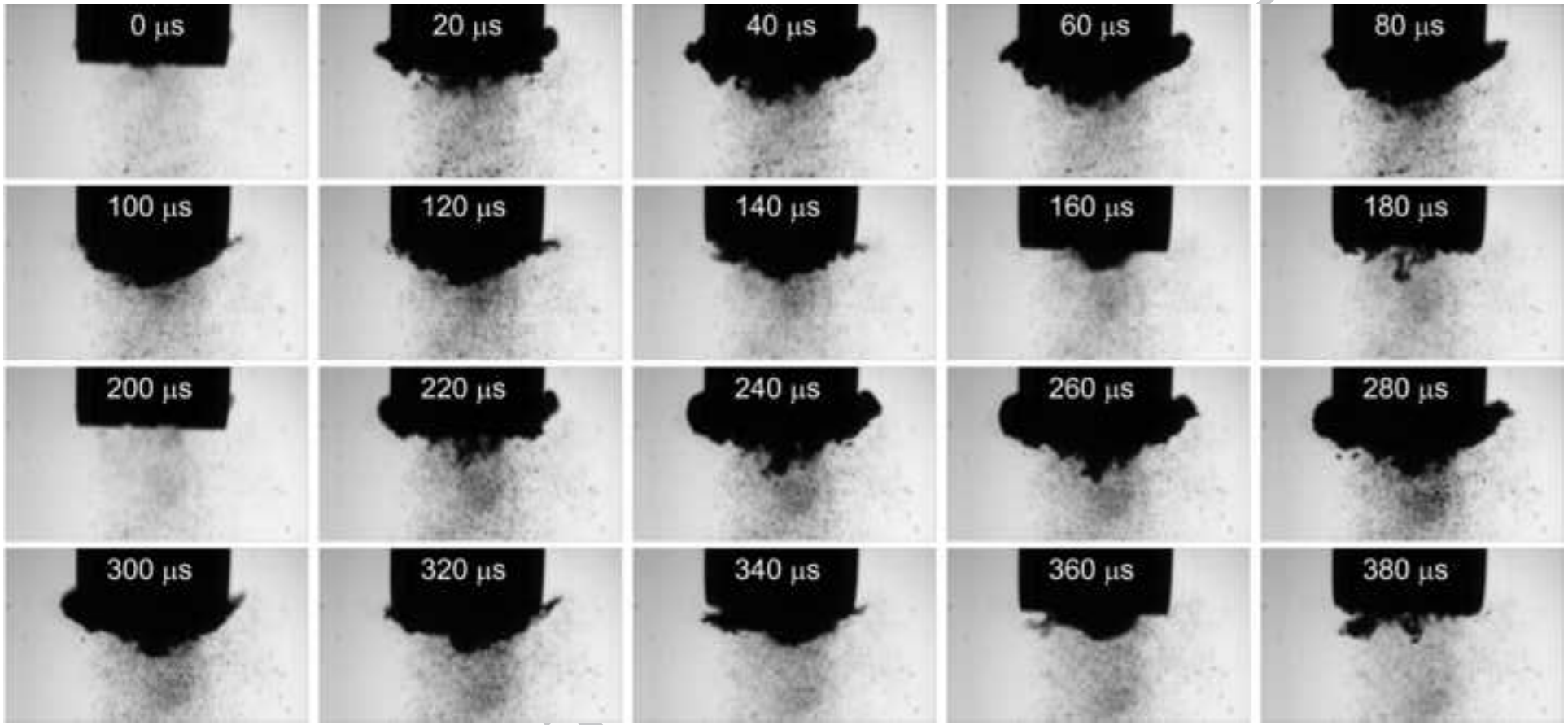

Figure02

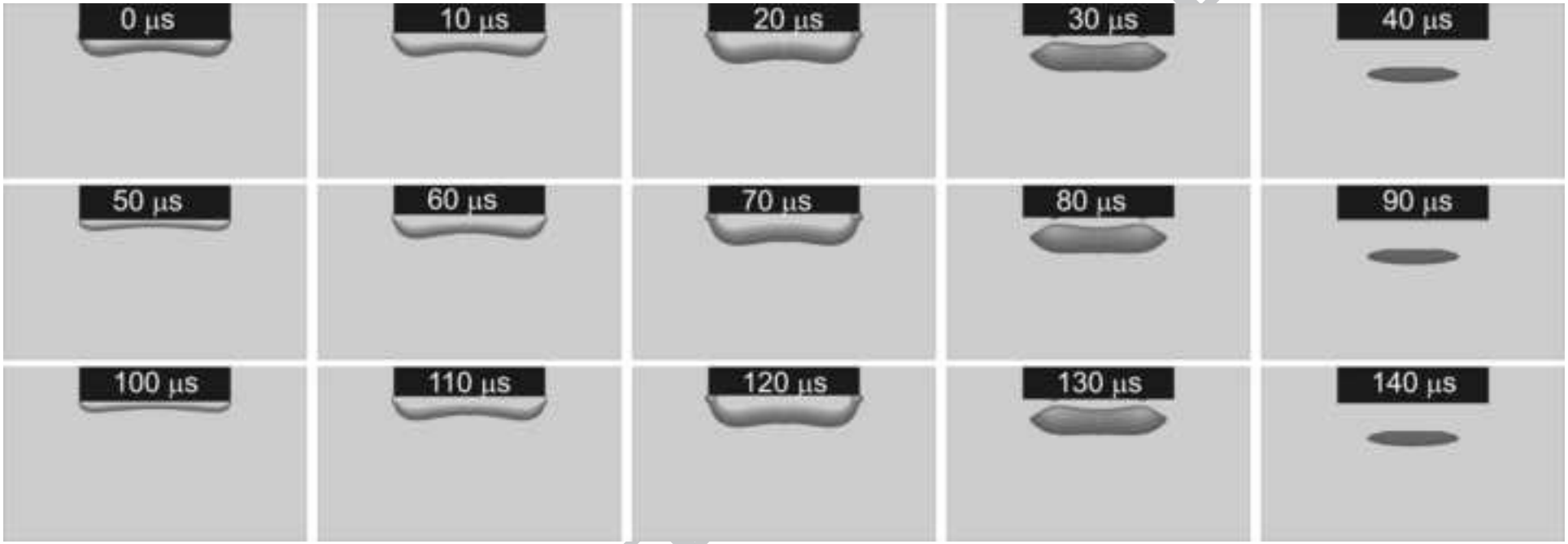

Figure03

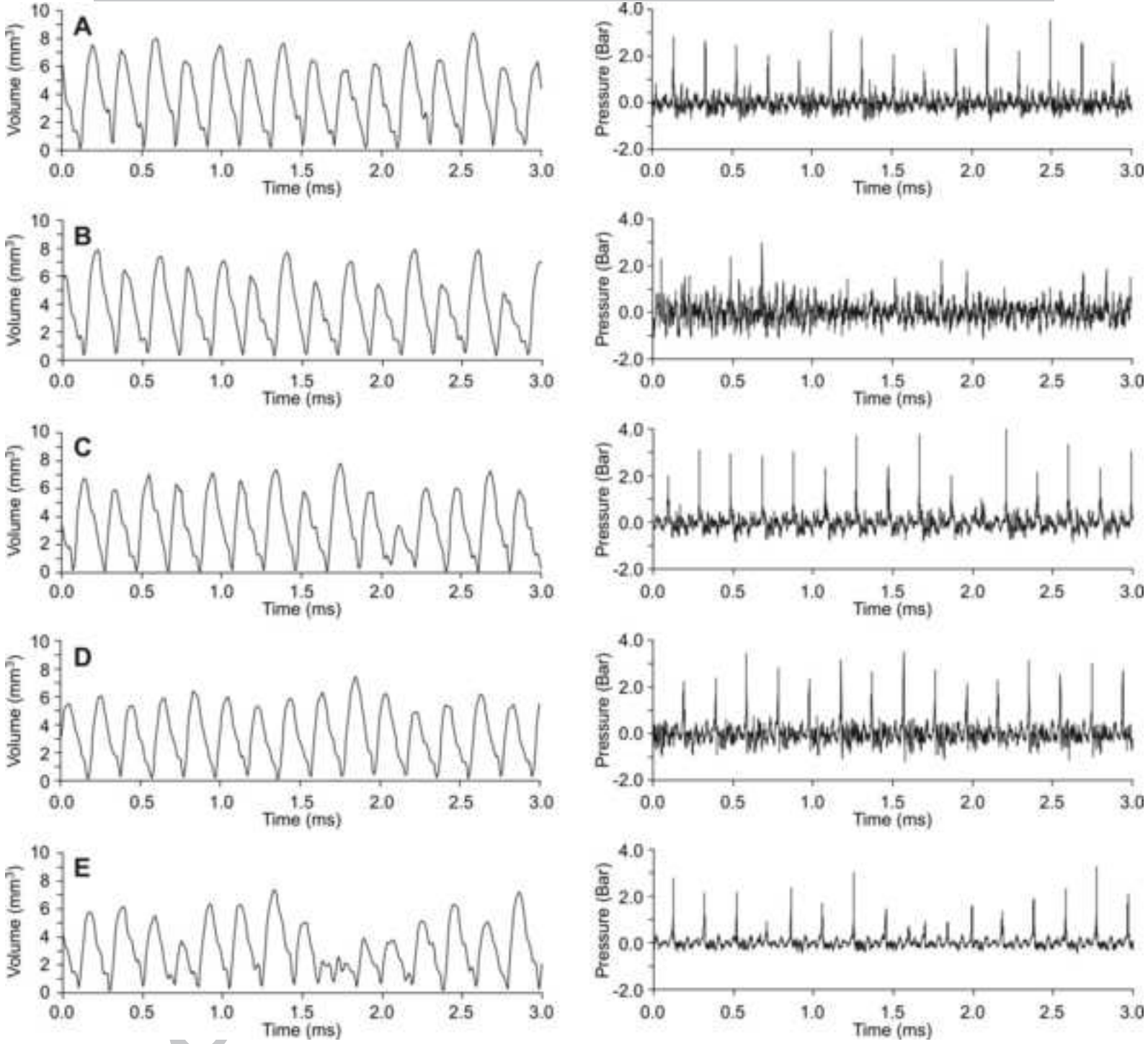

Figure04

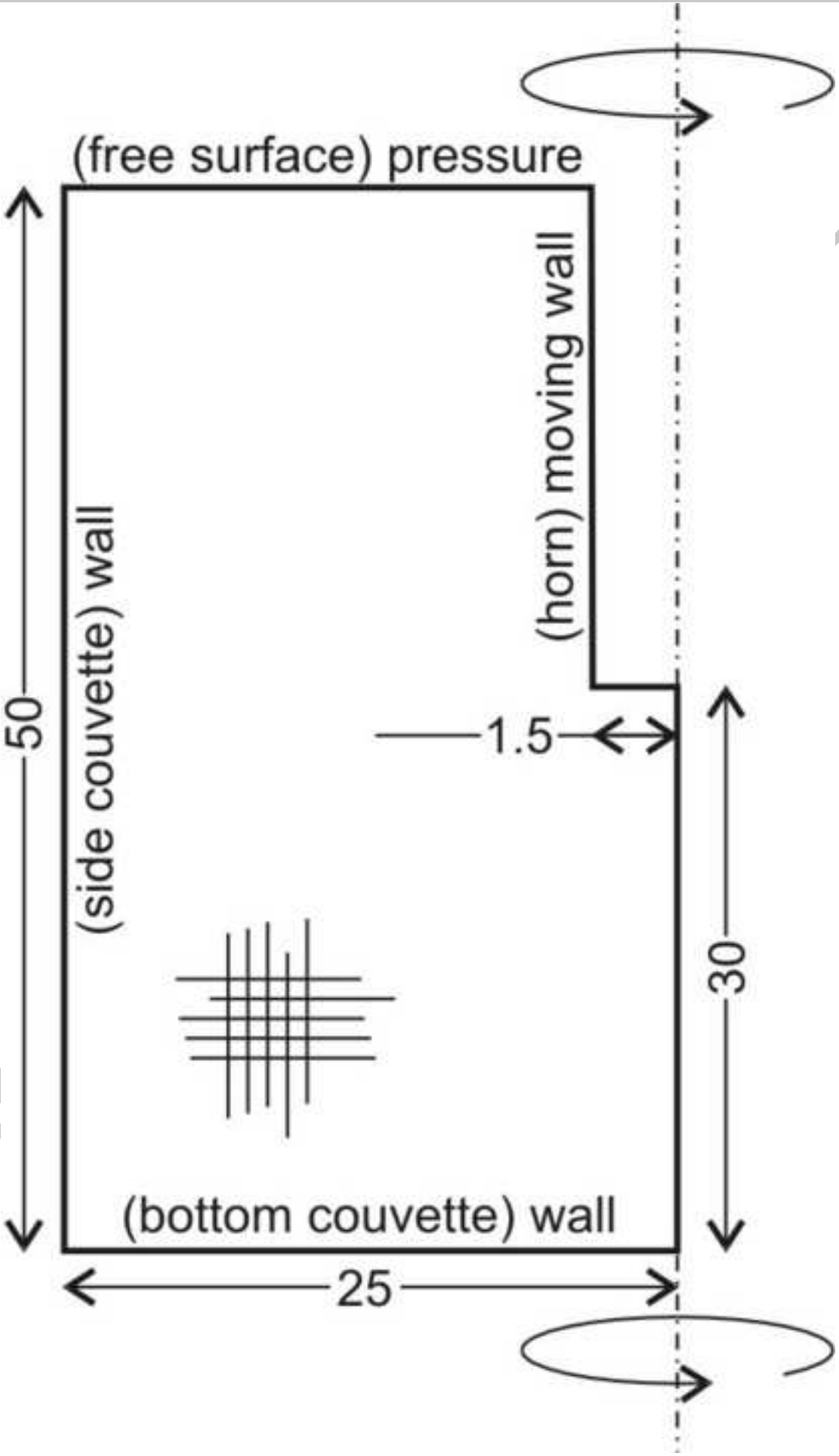

Figure05

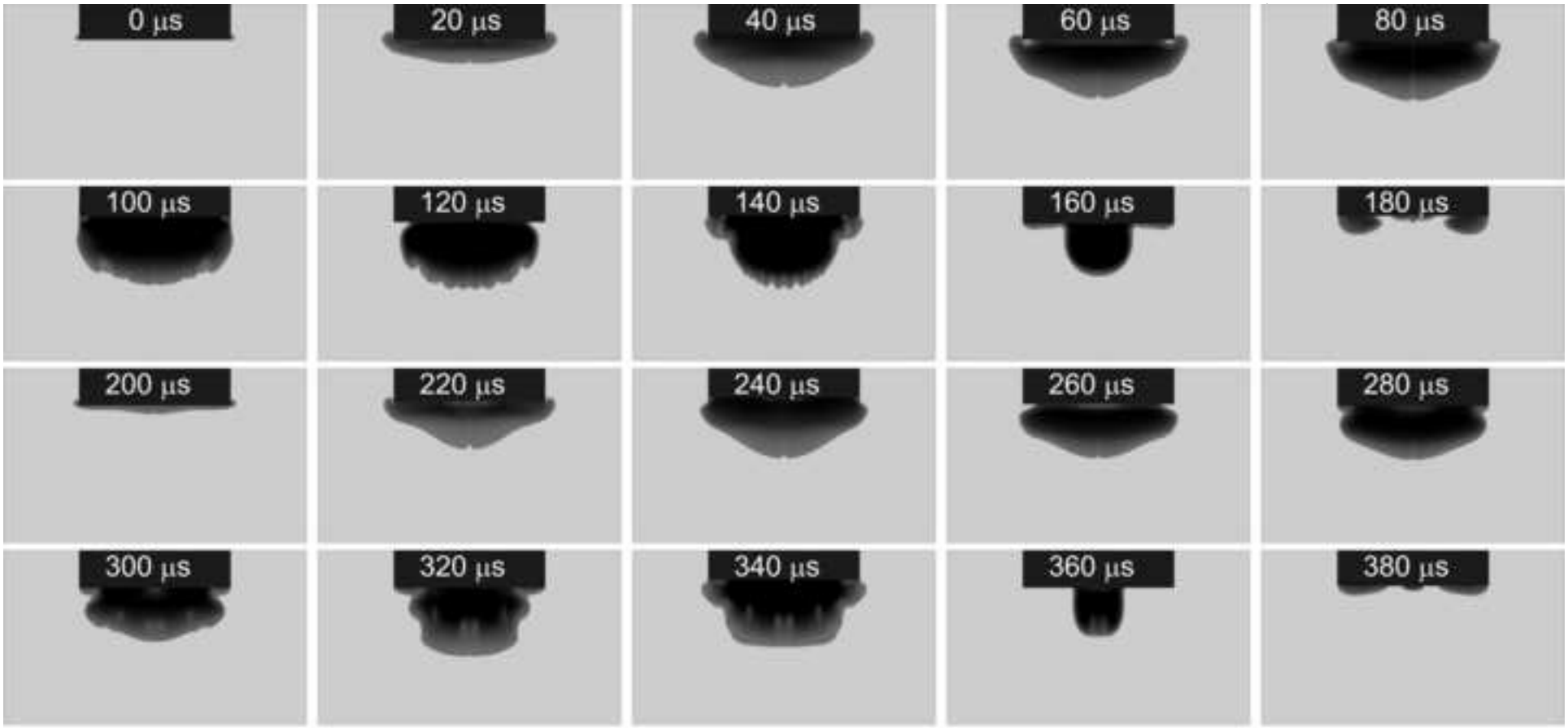

Figure06

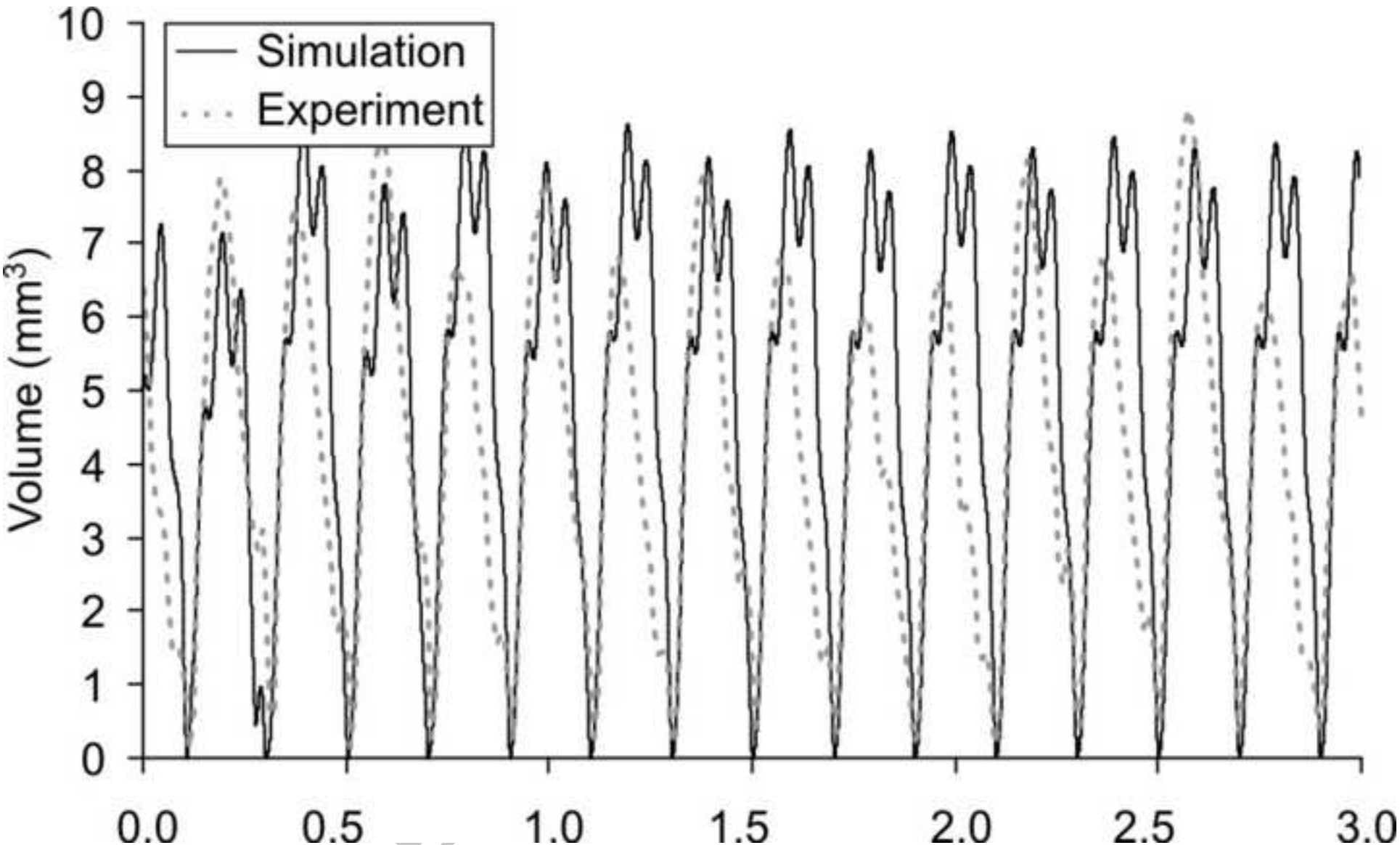

Figure07

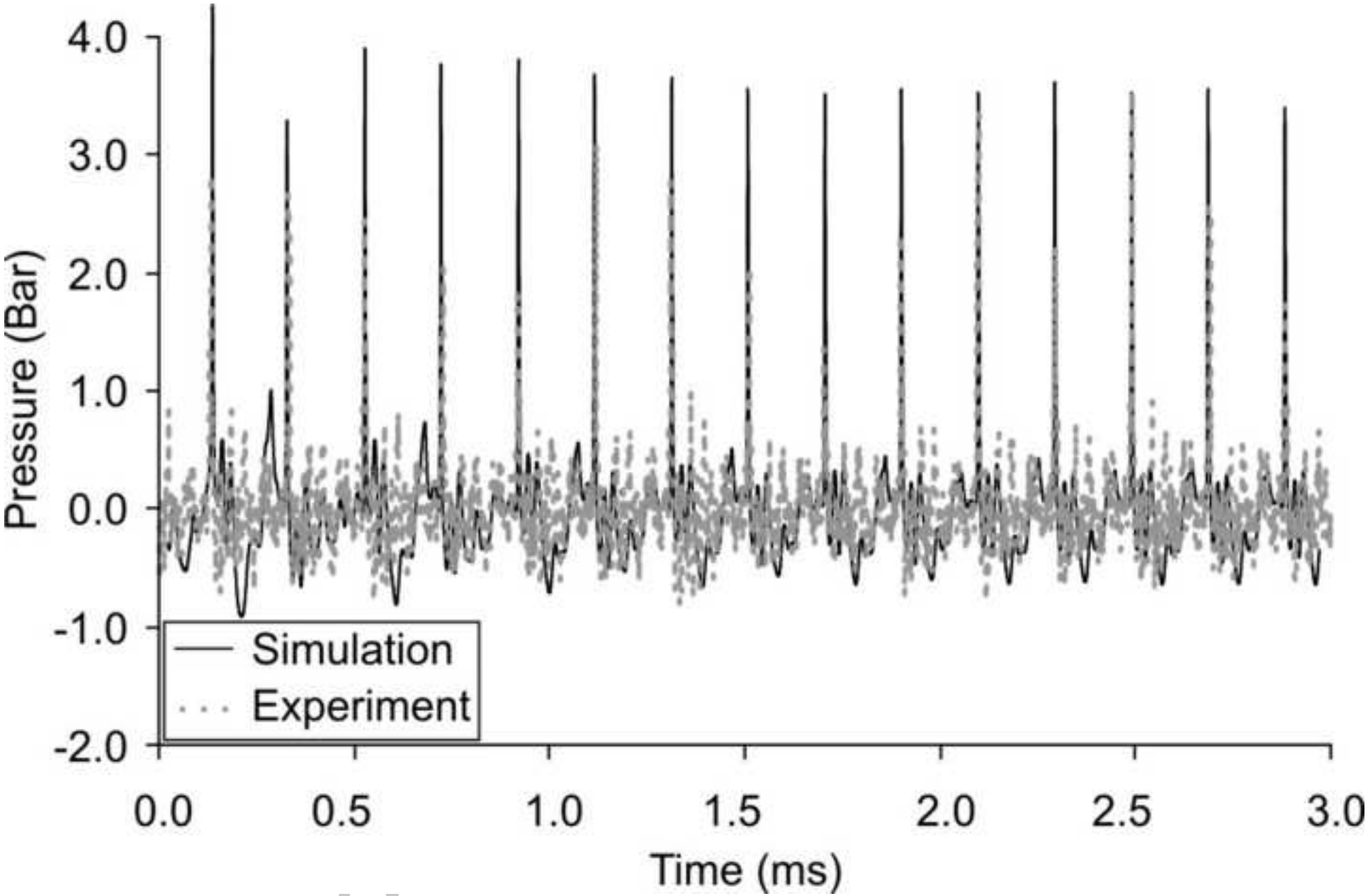

Figure08

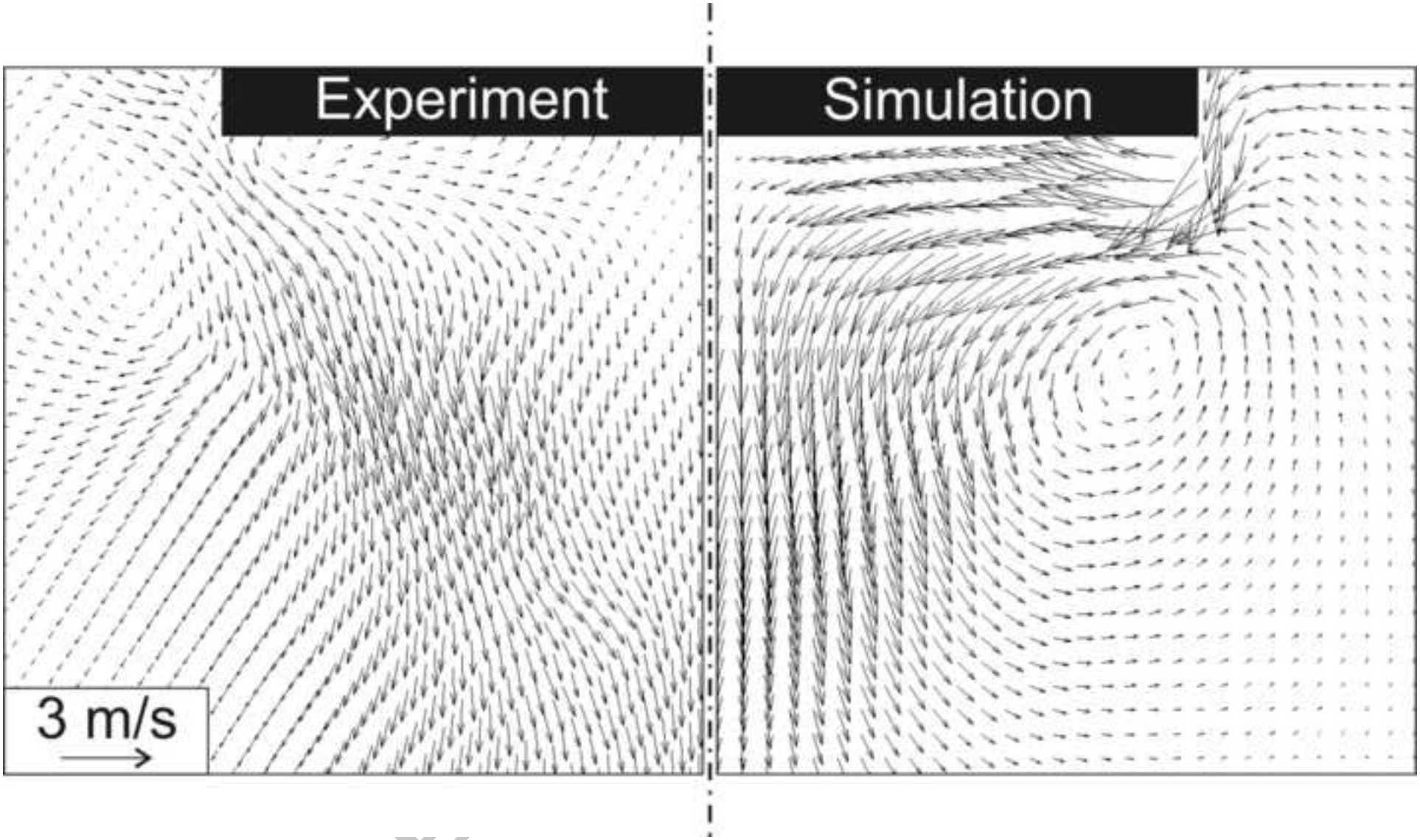

Figure09